Growth of doped PbS:Co^{2+} nanocrystals by Chemical Bath

O. Portillo-Moreno[a,*], R. Gutiérrez-Pérez[a], M. Chávez Portillo[a], M.N. Márquez Specia[a], G. Hernández-Téllez[a], M. Lazcano Hernández[a], A. Moreno Rodríguez[a], R. Palomino-Merino[b], E. Rubio Rosas[c]

[a]*Materials Science Laboratory, Fac. Ciencias Químicas, Universidad Autónoma de Puebla, P.O. Box 1067, Puebla, 72001, Pue. México.*

[*] *e-mail: osporti@yahoo.com.mx*

[b]*Fac. Ciencias Físico Matemáticas, Posgrado en Física Aplicada, Universidad Autónoma de Puebla, México, 72001.*

[c]*Centro Universitario de Vinculación y Transferencia de Tecnología, Universidad Autónoma de Puebla, Ciudad Universitaria, 72001.*

Received 12 October 2015; accepted 13 May 2016

Nanocrystalline PbS films grown by chemical bath at $T = 40 \pm 2$ °C onto glass slides were modified by in situ Co^{2+} -doping and their structural and optical properties were examined. By FT-IR spectra, a sharp stretching mode can be seen at ~ 1384 cm^{-1} due to the vibration mode of CO_3^2 ions. XRD patterns shown the growth on the zinc blende crystalline face. The grain size was determined by using X-rays diffractograms and was found at ~ 28 nm and $\sim 13 - 25$ nm for undoped and doped samples, respectively. Optical absorption spectra was used for calculating the energy band gap, and displayed a shift in the $\sim 1.21 - 2.21$ eV range, associated with quantum confinement effect. Raman peaks at ~ 210, 271, and 451 cm^{-1}, corresponding to a 1LO phonon mode, a two-phonon process, and a 2LO phonon mode respectively were also recorded. The surface and grain size of the films were measured by AFM studies.

Keywords: Thin films; nanocrystals; quantum; confinement effect; doping.

PACS: 71.20.Nr; 68.55.A; 64.70.kg

1. Introduction

Semiconductors obtained by combining elements from IIB and VA groups, such as CdSe, CdS, PbS, ZnO, etc., are interesting systems demonstrating quantum-confinement effects as the nanocrystal size corresponds to the Bohr exciton radius. Some reports have evidenced that quantum confinement in thin films produced by reduction grain size (GS) afford changes in electro-optical properties that can be exploited in a broad range of applications [1]. Hence, doping of semiconductors have shown different optical and structural changes in Lead Chalcogenide materials. Furthermore, there is an increasing interest into deposition of ternary derivative materials due to their potential tunable band-gap energy (E_g), by means of the growth parameters such as reaction temperature and concentration of reactive precursors by systematic doping [2,3]. Several methods for the preparation of PbS nanocrystals have been reported in recent years such as microwave and sonochemical methods [4], chemosyntesis [5], etc. However, most of the reported studies have been focused on the deposition of ternary derivatives material on thin films as $Pb_{1-x}Co_xS$ [6], $Pb_{1-x}Ni_xS$ [7], $Pb_{1-x}Cd_xS$ [8]. In this regard, PbS nanocrystals with GS dimensions in the 5-20 nm range are of technological interest for advanced optoelectronic applications, showing a stronger quantum confinement effect when the crystal size matches the dimension of Bohr exciton [9]. In the present work, PbS and PbSCo^{2+}-doped films were prepared by a green approach: chemical bath (CB), in order to investigate their structural and optical properties. FTIR spectra were recorded using a Perkin Elmer spectrophotometer in the 500-4000 cm^{-1} wavelength region. The crystalline structure characterization was carried out by X-Ray diffraction (XRD) patterns registered in a Bruker D8 Discover Diffractometer, using the Cu Kα line. The optical absorption spectra, measured in a Varian CARY spectrophotometer, allowed to calculate E_g. A micro-Raman Lab Ram-Idler apparatus with an excitement line of 514.5 nm wavelength Ar laser for Raman spectroscopy was used. Images of the surface were obtained by atomic force microscopy (AFM) with Nano-scoped E model contact mode instrument from UGC-DAE consortium of Scientific Research, Indore.

2. Chemical reactions and experimental procedure

We carried out a simple model of chemical reactions in the preparation of undoped and doped PbS films with a Co^{2+} solution determined by employing the reported cell potential values in basic media [7,10,11]

$$SC(NH_2)_2 + 3OH^- \leftrightarrow CO_3^{2-} + S^{2-} + 7H^+ \qquad (1)$$

$CH_3\,COO^-$ ion is generated by dissociation of $Pb(CH_3CO_3)$ according to:

$$Pb(CH_3COO)_2 \leftrightarrow Pb^{2+} + 2CH_3COO^- \qquad (2)$$

The coordinate complex ion $[Pb(NH_3)_4]^{2+}$ generated inderectly in our working conditions slowly release Pb^{2+} ions [7]:

$$[Pb(NH_3)_4]^{2+} + S^{2-} \leftrightarrow PbS + 4NH_3$$

$$\Delta G^0 = +362.88 \quad \text{KJ} \qquad (3)$$

The doping that generates Co^{2+} ion has the following chemical equilibrium:

$$Co(OH)_2 \leftrightarrow Co^{2+} + 2OH^- \quad \Delta G^0 = +140.08 \text{ KJ} \quad (4)$$

Finally, the overall reaction is:

$$[Pb(NH_3)_4]^{2+} + S^{2-}Co(OH)_2 \leftrightarrow PbSCo^{2+} + 4NH_3 + 2OH^- \quad \Delta G^0 = +502.96 \text{ KJ} \quad (5)$$

Chemical equilibrium is associated with changes in Gibbs free energy as the dopant ion is incorporated in ionic form in the PbS samples.

For the preparation of polycrystalline PbS thin films onto glass substrates, both undoped and doped samples (volume-solution $V_{[Co^{2+}]}$ containing the doping Co^{2+} chemical agent) grown by CB, PbS films three different levels of doping $V_{[Co^{2+}]}$ were obtained by *in situ* addition of 10, 20, 30, mLs in the solution for PbS growth: $Pb(CH_3CO_3)_2$ (0.01M), KOH (0.1M), NH_4NO_3 (1.2M), $SC(NH_2)_2$ (0.1M). The solutions were mixed and the final solution kept at 40 ± 2 °C during 1.0 h [3]. The optimal doping concentration $V_{[Co^{2+}]}$ $Co(NO_3)_2$ (0.125 M) was determined after several trials when the films had attained good adherence. This solution is routinely added to the reaction mixture during the growth of the PbS films. The samples were labelled as PbS for the undoped sample and PbSCo10,..., PbSCo30 for the doped samples.

3. Results and discussion

FT-IR spectra of PbS and $PbSCo^{2+}$ -doped films are displayed in Fig. 1. The main spectral features are similar, excepting the intensity of the absorption band of CO_3^{2-} at $\sim$1384 cm^{-1}; the band located at $\sim$1921 cm^{-1} was assigned to one of the fundamental frequency of COO^- bonds [12] (see equations (1) and (2) for the processes involved in the COO^- and CO_3^{2-} formation). The broad absorption band at the $\sim$3423 cm^{-1} region can be attributed to stretching of the

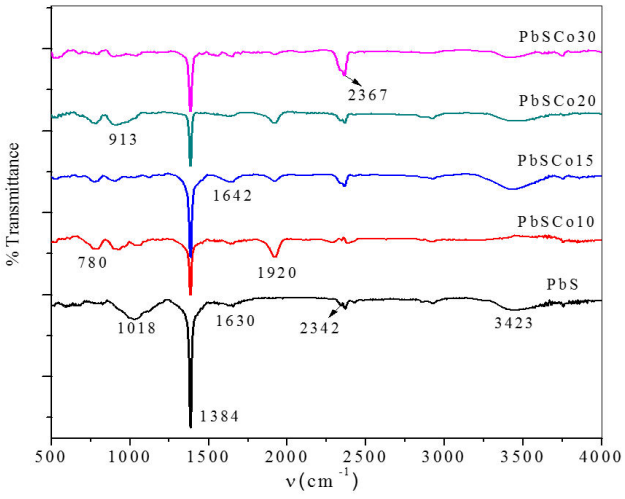

FIGURE 1. FT-IR spectra of PbS-PbSCo nanoparticles.

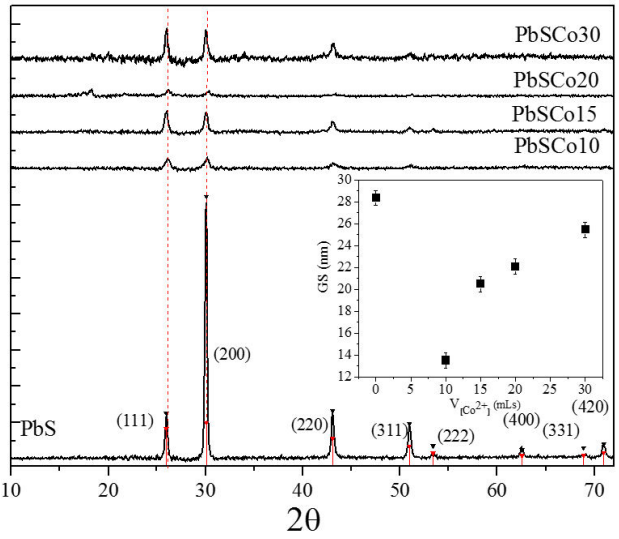

FIGURE 2. X-ray diffractograms for PbS-PbSCo30 films. Inset shows Average grain size (GS) vs. $V_{[Co^{2+}]}$ of PbS-PbSCo films.

-OH groups of defective sites and the physically adsorbed water molecules. The bands at $\sim$ 1642 and $\sim$ 1018 cm^{-1} were ascribed to the vibration of amine groups [13]. The peak at $\sim$2342 and $\sim$2367 cm^{-1} are characteristic of COO^- and S-H stretching vibrations, confirming the presence of acetate and sulfur ions. The decrease in the peak located at $\sim$1384 cm^{-1}, assigned to the CO_3^{2-} vibration indicates the bonding to the surface of PbS by the carboxyl groups. As a result, the characteristic vibrations for the CO_3^{-2} ions displayed at 1642 cm^{-1} and 1630 cm^{-1} are symmetric bending and stretching modes, respectively. The Pb-S bond is mainly an electrovalent bond, thus the FT-IR spectrum of spectrum

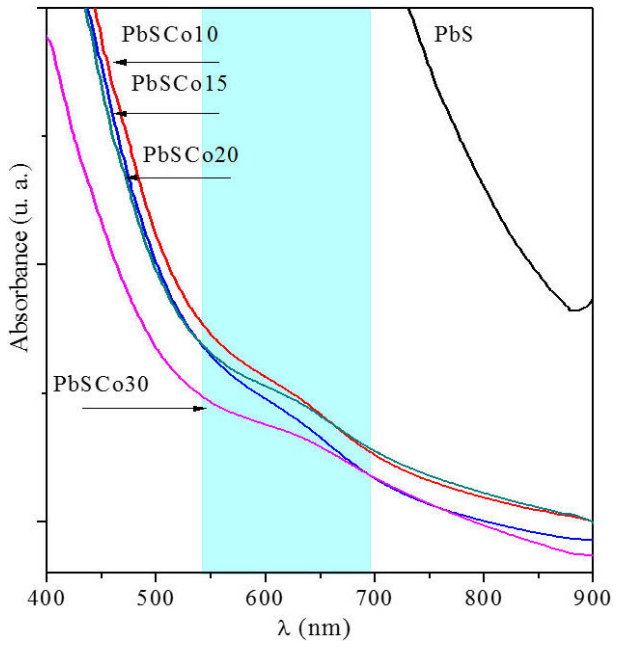

FIGURE 3. Absorbance spectra of PbS-PbSCo films.

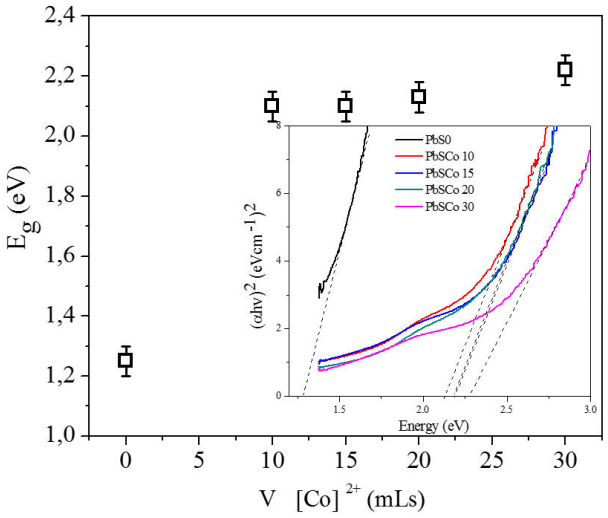

FIGURE 4. Graph of E_g vs. $(\alpha h\gamma)2$ PbS-PbSCo samples. Inset shows plot of E_g vs. $V_{[Co^{2+}]}$ PbS-PbSCo layers.

of PbS does not show strong bands associated with Pb-S stretching and bending vibration. The bands at ~ 780 and ~ 920 cm^{-1} were not identified, but may be associated with Pb-Co bonds. When $V_{[Co^{2+}]}$ is added and PbS are supplied into crystals, the interactions reduce as some of PbS will react to forms nanoparticles. A comparison of these spectra clearly shows that many CH_3-COO^-, OH^- and CO_3^{-2} ions remain on the surface of nanocrystals, which were removed by washing with distilled water and drying the films with an hot air flow.

We associate this peak broadening considering the Pb^{2+} ion radius compared to the dopant ionaccording to: Pb^{2+} = 1.20 Å, S^{2-} = 1.84 Å and Co^{2+} = 0.83 Å. In a previous report [7], we proposed the following that for a relative low concentration of Co^{2+} ions, a majority can be located in (i) Pb^{2+} vacancies sites, which otherwise would be empty (ii) in Pb^{2+} sites causing the appearance of Pb^{2+} interstitial sites, and (iii) in interstitial positions [3]. It can be mentioned that the stable crystal structure of PbS, when Co^{2+} occupies more sites of Pb^{2+} in the host lattice, afford an increase in internal strain. Through this gradual occupation in vacancies and interstitial sites of the ions in the crystal lattice, the GS is reduced to release the strain. As the Co^{2+} concentration is increased, the diffraction peaks become broader due to the reduction in the GS. Inset in Fig. 2 shows the GS vs $V_{[Co^{2+}]}$ for all samples corresponding to the (200) plane. The GS of ~ 28 nm for PbS and PbSCo10 layers decrease ~ 13 nm, however GS increase almost linearly with increasing $V_{[Co^{2+}]}$. The effect of the GS by the doping effect has been reported in films of doped samples [2,3,5].

The absorbance spectra vs wavelength (nm) of all the films is shown in Fig. 3, in order to compare the changes produced by the dopant. These absorption spectra show an abrupt change in the doped samples compared to undoped PbS. The spectra of PbSCo20 and PbSCo30 layers exhibited an absorption onset of $\sim 550 - 700$ nm, these bands are shown with a blue strip. These exciton bands were attributed to a $^1S_e - ^1S_h$ transition, this effect is associated with quantum confinement produced by the decrease of GS [14]. However, Todd *et al*. reported three sharp peaks in the absorption spectra of the lowest exciton transitions calculated for particles of 1.5 nm radius [15]. The absorption spectra in the visible light region presents a component at ~ 587 nm, assigned to the spin and electric-dipole-allowed $^4A_2(F) \rightarrow {}^2A_1(G)$, $^4A_2(F) \rightarrow {}^2T_1(G)$, and $^4A_2(F) \rightarrow {}^2E(G)$ transitions, respectively. All doped samples have weak absorption in the visible and NIR regions, and the intensity of the absorption band increases with $V_{[Co^{2+}]}$ increasing. Such augmentation is associated with the increasing of Co^{2+} ions located in tetrahedral sites of PbS. The observed structures in the optical absorption spectra of PbSCo samples are similar to those observed in other materials, both in bulk as well as in the nanocrystalline form [16].

A comparison of the effect of nanocrystalline size on electron-phonon coupling for PbS quantum dots with controlled but variable particle size in PbSCo grown by CB has not been reported so far. The plot of E_g vs. $V_{[Co^{2+}]}$ for all samples is displayed in Fig. 4. It can be observed a $E_g = 1.21$ eV for the PbS sample. Bulk PbS ($E_g = 0.41$ eV) and bulk CoS ($E_g = 1.15$ eV) are expected to vary E_g between 0.41 and 1.15 eV, however in these spectra such change are not appreciated [6]. The confinement effect appears as a shift in the edge of the absorption spectra and the absorption to lower wavelengths, due to the decrease in GS and number of defects. It is clearly seen, from the optical spectrum, an absorption edge shift towards a lower wavelength in doped films. Thus, the observed modification of PbSCo samples showed the existence of quantum confinement. The experi-

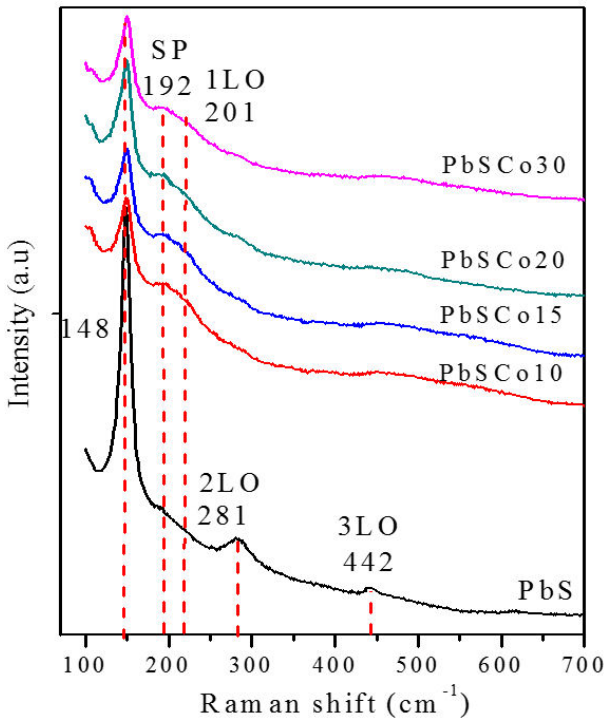

FIGURE 5. Raman spectra of PbS-PbSCo films.

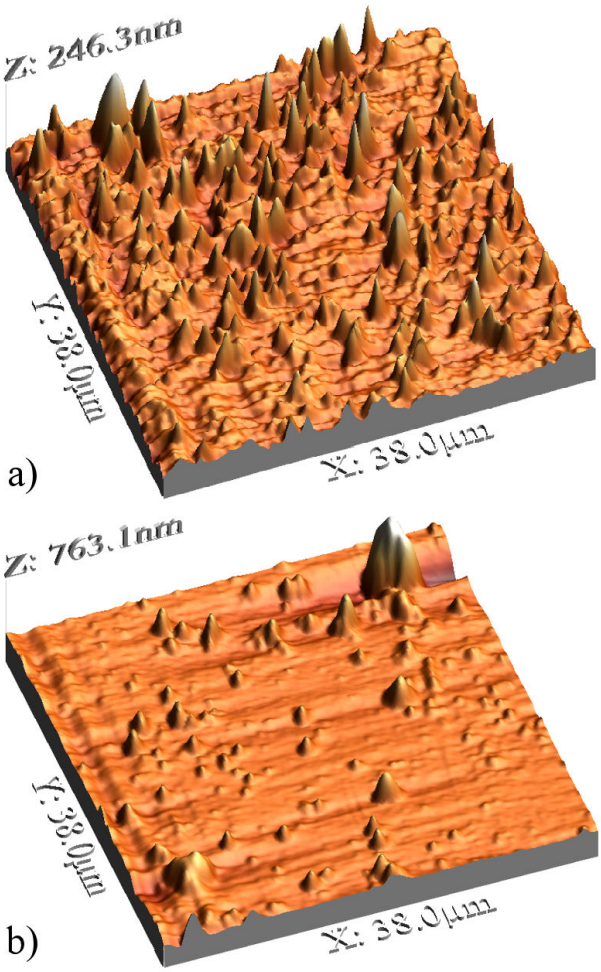

FIGURE 6. 3D AFM images of nanocrystalline (a) PbS, (b) PbSCo30.

mentally observed E_g values for the shift indicated an alloying in nanocrystalline PbS [17,18]. The fundamental optical transition of doped films ($E_g = 0.41$ eV) is not observed in these doped films, because of complete mixing of PbS with Co^{2+} ions yielding an unique intermetallic compound of $Pb_xCo_{1-X}S$ type [5]. The E_g in our work for samples in the $\sim 1.2 - 2.2$ eV range shows the extent of quantum size effect in the nanoparticle films. A similar shift observed in the position of the excitonic peak towards higher energies in CdSe crystallites has been explained due to a decrease in crystallite size [19]. Inset in Fig. 4 shows the plot of E_g vs. $(\alpha h\gamma)^2$ of PbS-PbSCo. In our case, the introduction of Co^{2+} ions into the PbS lattice induced a increase of strain. Such strain in PbSCo samples tends to reduce GS.

Raman spectra is shown in Fig. 5. The spectra are compared each other to observe the differences produced by the Co^{2+} dopant. Similar peaks in these spectra at 148, 192, 201, 281, 442 cm^{-1} are observed along with a prominent band at ~ 148 cm^{-1}. Peaks at ~ 210, 271, 451 cm^{-1} can also be observed, corresponding to a 1LO phonon mode, a two-phonon process, and a 2LO phonon mode, respectively [20]. In addition, the peak or shoulder at ~ 192 cm^{-1} has been identified to be due to the SP mode, and its intensity greatly increases with decreasing crystal size.

These results confirm those obtained by optical absorption and XRD. They are influenced by some parameters, such as atomic masses of Pb, S and Co atoms and vibration constant of bonding atoms residing in the lattice. Our measurements on samples from different $V_{[Co^{2+}]}$ exhibited a variation on the intensity of these broad bands, so in these films, the effect of dopant is clear and can be seen with variations of the intensities of the bands. The reason for this behavior is associated with the stoichiometry of PbS caused by the gradual incorporation of the Co^{2+} ions. Raman bands in the high-frequency two-phonon region can also be observed at ~ 450 cm^{-1} [7].

The 3D images of atomic force microscopy (AFM) are showed in Fig. 6 for: (a) PbS, in this image the surface morphology exhibited agglomerates with pyramidal geometry grown on the flat surface, and no holes or islands are observed. (b) in this 3D image of PbSCo20 film, the disappearance of conglomerates displayed an almost flat surface. In this sample the effect of dopant can be clearly seen. Images of all doped samples are not shown because there are few significant changes compared to the one shown here.

4. Conclusions

The effect of $V_{[Co^{2+}]}$ on the morphological, crystal structure and optical band gap properties of thin films has been investigated. The composition study showed that these films were stoichiometric, with slight variation in sulfur deficiency. The XRD pattern revealed that films are crystalline with average grain size decreased as $V_{[Co^{2+}]}$ increased. These films also displayed large final thickness and their surface morphologies were composed of small grains with an approximate size of 27-12 nm. Optical absorbance measurements indicated the existence of direct transition with corresponding energy gap in a 2.1-2.4 eV range. These films also exhibited a good transmittance of about 60% in visible and near infrared regions, allowing their potential use as a window layer in high efficiency thin films solar cells. In summary, we have found an efficient process to introduce Co^{2+} ions into the PbS structure with, practically, no large damage to the lattice.

Acknowledgments

The authors thank Lic R. Villegas Tovar from BUAP Library from their collaboration in the achievement of this research.

1. E.O. Chukwuocha, M.C. Onyeaju, T.S.T. Harry, *Condensed Matter Physics* **2** (2012) 96-100.
2. K. Rakesh, H.A. Joshi, H.K. Sehgal, *Appl. Surf. Sci.* **14** (2003) 809.
3. R. Palomino Merino *et al*., *J. Nanosci. Nanotech.* **14** (2014) 5408.
4. H. Khallaf, C. Guangyu, O. Lupan, L. Chow, S. Park, A. Schulte, *Appl. Surf. Sci.* **255** (2009) 4129.
5. S.B. Pawar, J.S. Shaikh, R.S. Devan, Y.R. Ma, P.N. Bhosale, P.S. Patil, *Appl. Surf. Sci*. **258** (2011) 1869.
6. N. Mathur, R.K. Joshi, G.V. Subbaraju, H.K. Sehgal, *Physica B* **23** (2004) 56.
7. O. Portillo Moreno *et al*., *ISRN Nanotechnology*, **1** (2012).
8. H.M. Upadhyaya, S. Chandra, *J. Mat. Sci* **29** (1994) 2134.
9. J.B. Biswal, N.V. Sawant, S.S. Garje, *Thin Solid Films* **518** (2010) 3164.
10. A.J. Bethune, N.A.S Loud. In Standard Aqueous Potential and Temperature Coefficients at 25°C, C.C. Hampel, Skokie, II. 1969.
11. M. Chávez Portillo *et al*., *Rev. Mex. Fis.* **61** (2015) 83.
12. C. Li, Y. Zaho, F. Li, Z. Shi, S. Feng, *Chem. Mat.* **22** (2010) 1901; Froment, M. Lincot, *D. Electrochem. Acta* **40** (1995) 1293.
13. D.H. Lee, R.A. Condrate, J.S. Reed, *J. Mater. Sci.* **31** (1996) 471.
14. Y. Wang, A. Suna, W. Mahler, R. Kasowsky, *J. Chem. Phys.* **87** (1987) 7315.
15. F.J. Torres, U.R. Rodríguez Mendoza, V. Lavin, E.R. de Sola, J. Alarcón, *J. Non-Cryst. Solids* **353** (2007) 4093.
16. L. Nataf, F. Rodríguez, R. Valiente, *Phys. Rev. B* **86** (2012) 10010.
17. R. Kostic *et al*., *Opt. Mat.*, **30** (2010) 1177.
18. M.J. Ventura, C. Bullen, M. Gu, *Opt. Express* **15** (2007) 1622.
19. A. Rivera Márquez *et al*., *phys. solidi state* **188** (2001) 1059.
20. J.P. Ge, J. Wang, H.-X. Zhang, X. Wang, Q. Peng, Y.-D. Li, *Chem. Eur. J.* **11** (2005) 1889.